Heliyon 10 (2024) e39255

Contents lists available at ScienceDirect

Heliyon

journal homepage: www.cell.com/heliyon

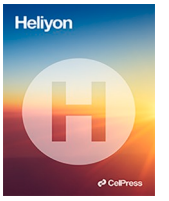

Research article

Plant-mediated synthesis of zinc oxide (ZnO) nanoparticles using *Alnus nepalensis* D. Don for biological applications

Dipak Raj Jaishi [a], Indra Ojha [a], Govinda Bhattarai [a], Rabina Baraili [a], Ishwor Pathak [b], Dinesh Raj Ojha [a], Deepak Kumar Shrestha [a,c], Khaga Raj Sharma [a,*]

[a] *Central Department of Chemistry, Tribhuvan University, Kirtipur, Kathmandu, Nepal*
[b] *Department of Chemistry, Amrit Campus, Tribhuvan University, Kathmandu, Nepal*
[c] *Department of Chemistry, Butwal Multiple Campus, Tribhuvan University, Nepal*

ARTICLE INFO

Keywords:
Alnus nepalensis D. Don
Antimicrobial
Antioxidant
Green synthesis
MBC
MIC
Toxicity
Zinc oxide nanoparticles

ABSTRACT

An aqueous bark extract of *A. nepalensis* D. Don was utilized to prepare zinc oxide (ZnO) nanoparticles through a green method, which is more economical, eco-friendly, and effective for exploring several biological applications and toxicity assessments against brine shrimp nauplii. The prepared ZnO nanoparticles were characterized using several characterizing techniques. The surface morphology and the elemental composition of the prepared ZnO NPs was analyzed by field emission scanning electron microscopy (FE-SEM), and energy dispersive X-ray (EDX) analysis. The colour of the solution was changed from reddish-brown to white indicating the formation of ZnO NPs which shows UV–vis absorption at 361 nm. The various functional groups of the organic compounds present in plant extract act as reducing and stabilizing agents in the formation of nanoparticles. The involvement of these functionalities in the formation of nanoparticles is indicated by the shifts and changes in the IR spectra of both the plant extract and the ZnO nanoparticles. The size of the nanoparticles was determined to be 15.31 nm with XRD analysis while the FE-SEM revealed the average grain size of 67.29 nm with irregular shape. The elemental composition of ZnO NPs shows a greater atomic percentage of zinc compared to other elements (C, N, Ni, O, and Ag), with an intense peak of zinc observed at approximately 1 keV. The trace amount of silver is due to the impurities present in the reagent used in the experiment. The antioxidant property of ZnO nanoparticles was evaluated with an IC_{50} of 53.02 ± 3.43 μg/mL. The ZnO nanoparticles exhibited significant antibacterial activity against *Klebsiella pneumoniae* and *Escherichia coli*, with zones of inhibition (ZOI) of 18 mm and 23 mm, respectively as compared to the positive control neomycin of ZOI 28 mm against *K. pneumoniae*. The potential antibacterial activity of the ZnO NPS was revealed as the MIC and MBC against *K. pneumoniae* of 0.39 mg/mL and 0.78 mg/mL, respectively. In addition, the prepared ZnO nanoparticles showed toxicity against brine shrimp nauplii of LC_{50} 16.59 μg/mL. The results of this study impart that plant-assisted synthesized ZnO nanoparticles possess significant antibacterial properties that reduce oxidative stress in human cells, ultimately contributing to cancer prevention.

* Corresponding author.
E-mail address: khaga.sharma@cdc.tu.edu.np (K.R. Sharma).

https://doi.org/10.1016/j.heliyon.2024.e39255
Received 25 July 2024; Received in revised form 8 October 2024; Accepted 10 October 2024
Available online 12 October 2024

1. Introduction

Alnus nepalensis D. Don, commonly known as Nepalese alder, belongs to the family Betulaceae. This species thrives in gully terrace forests and river beach wetlands across a wide elevation range of approximately 700–3600 m. It grows rapidly in warm, humid regions, potentially reaching a height of about 13 m within just five years [1]. Traditionally, *A. nepalensis* D. Don has been employed in traditional medicine to treat wounds, cuts, diarrhea, dysentery, and inflammatory diseases. It possesses various properties, including antioxidant, hepatoprotective, antidiabetic, antiobesity, and gastroprotective effects [2]. Nanotechnology encompasses the study of nanomaterials, specifically structures and chemicals at the nanoscale (1–100 nm). A diverse class of materials, known as nanoparticles (NPs), has a size of 1–100 nm [3]. Various methods are available for synthesizing nanoparticles, especially those utilizing noble metals [4–9]. Plant-mediated synthesis of nanoparticles is increasingly employed for its reduced toxicity, lack of hazardous chemical byproducts, and eco-friendly nature [10].

The biological method is widely recognized for producing stable, nontoxic, and environment-safety nanoparticles [11,12]. The physical and chemical methods often yield hazardous nanoparticles, leading to significant environmental concerns. Additionally, the reducing or capping agents used in chemical and physical processes can be expensive. Consequently, the synthesis of nanoparticles assisting plant extracts is preferred, as these extracts can stabilize nanoparticles and reduce metal ions [13]. This biological method is advantageous because it utilizes biological components, such as yeast, fungi, bacteria, and plant secondary metabolites, as precursors for synthesis [4,6].

Plant-mediated synthesized ZnO NPs exhibit novel physicochemical characteristics and have diverse biological applications, including wound healing, antimicrobial, antiviral, antidiabetic, antioxidant, and antifungal properties [14–18]. ZnO NPs possess distinct chemical, optical, and electrical properties, making them highly sought after for use in various electronic devices [19]. Zinc is a vital element in the human body, found in hard tissues such as teeth, muscles, bones, and skin. Their optical, morphological, catalytic, magnetic, electrical, mechanical, and photochemical properties underscore the importance of synthesizing ZnO nanoparticles in the modern world. The properties of these nanoparticles can be tailored by altering their size or doping them with additional compounds [20] There is a significant correlation between the size, exposed surface area, band gap, and crystallinity of ZnO NPs, which contributes to their high conductivity [21], strong antibacterial potential, extended stability, improved electrical and thermal capabilities, and enhanced photocatalytic properties [22]. ZnO NPs are also noted for their high microbial resistance [23].

Phytochemicals such as anthocyanidins, flavonoids, tannins, and phenolic acids, which are examples of polyphenols, act as stabilizing and capping agents in the formation of nanoparticles. These phytoconstituents not only facilitate the fabrication of nanoparticles but also play a crucial role in maintaining their geometry [24]. The formation of nanoparticles involves giving the complexes between hydroxyl-rich phenolic rings and Zn^{2+} ions. This method facilitates the hydrolysis of the intermediate chelated molecule, resulting in the formation of $Zn(OH)_2$, which is subsequently calcined at elevated temperatures to yield ZnO nanoparticles. The electrostatic interactions facilitate the growth of ZnO NPs [25–27].

Despite the extensive literature on the green synthesis of ZnO NPs using plant extracts, the specific application of *Alnus nepalensis* D.

Fig. 1. *Alnus nepalensis* D. Don fresh sample used in the study.

Don for this purpose, along with its biological applications, has not been thoroughly explored. This study focuses on synthesizing ZnO NPs using plant extracts, characterizing them, and evaluating their biological applications.

2. Materials and methods

2.1. Chemicals

The chemicals used in this study were: zinc nitrate, EDTA disodium salt dihydrate (SRL), boric acid, calcium chloride (fused), and sodium chloride (Merck), all of which were obtained from a local supplier. The DPPH reagent and quercetin (both from Merck) were utilized for antioxidant activity assays. Resazurin was sourced from LOBA CHEMI Pvt. Ltd. Additionally, Mueller Hinton Agar, Mueller Hinton Broth, Neomycin, and Nutrient Agar were acquired from HieMedia Pvt. Ltd.

2.2. Software used

For data processing and analysis Originpro 2024, and Microsoft Excel (the most recent version) were used. The Genes Microplate software was used for the data collection. Origin Pro 2024 and Image J software were used to calculate the crystallite size and grain size of ZnO NPs by using XRD data and FE-SEM images. GraphPad Prism (Version 8.0.2.263) was used to calculate IC_{50} shown by the zinc oxide nanoparticles.

2.3. Methods

2.3.1. Sample collection and identification

The bark of *A. nepalensis* D. Don was collected from the Far-Western region, Doti district (Sayal Gaupalika ward no. 2), Nepal growing at an altitude of 2000 m, latitude and longitude 29°15′ N and 80°57′ E respectively. The plant sample was collected in October 2023 and identified with the voucher specimen 01KATH163159. The photograph of *A. nepalensis* D. Don fresh sample is shown in Fig. 1.

2.3.2. Extraction of plant metabolites and synthesis of zinc oxide nanoparticles

2.3.2.1. Plant extract. Five grams of *Alnus nepalensis* D. Don powder were dissolved in 100 mL of distilled water in a conical flask. The mixture was heated for 1 h at 50 °C on a hot plate using a magnetic stirrer. After heating, the resulting content was filtered and cooled. The filtrate was then stored at 4 °C for future use [28].

2.3.2.2. Synthesis of zinc oxide nanoparticles (ZnO NPs). ZnO NPs were synthesized using a combination of plant extract and a 0.15 M zinc nitrate solution at varying ratios of 1:15, 1:20, and 1:25. The optimal ratio for stability was determined through UV–vis spectroscopy, analyzing the mixtures. The results indicated that the most stable nanoparticles were obtained at the 1:20 ratio, achieved by mixing 10 mL of the aqueous plant extract with 200 mL of the 0.15 M zinc nitrate solution. Initially, the pH of the aqueous extract was

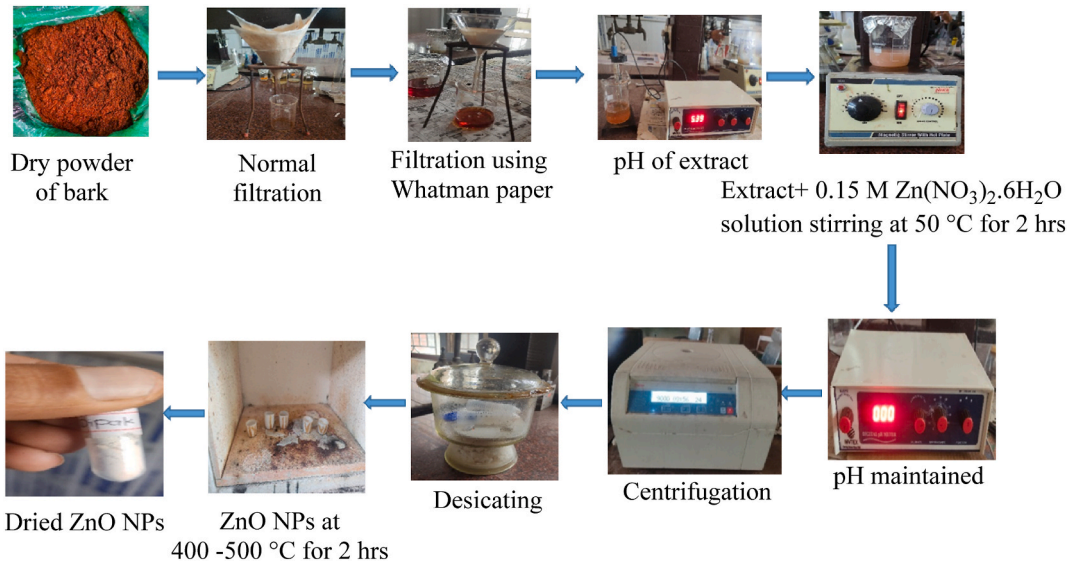

Fig. 2. Diagrammatic representation for the plant-assisted synthesis of ZnO NPs.

recorded at 5.39. To create a suitable environment for the synthesis, the pH of the solution was adjusted to 12 by incrementally adding zinc nitrate. The stability of the synthesized ZnO NPs was evaluated at three-time points: 0 h, 24 h, and 72 h. The presence of zinc oxide nanoparticles was visually indicated by the formation of a light white suspension. To isolate and purify the nanoparticles, the mixture was centrifuged at a speed of 9000–10,000 rpm for 1 h. This centrifugation was followed by thorough washing with ethanol and distilled water [29]. The resulting nanoparticles were then dried in a desiccator. For further purification, they were subjected to a muffle furnace at temperatures ranging from 400 to 500 °C for 2 h [30]. The synthesized ZnO nanoparticles were stored at 4 °C to minimize the risk of agglomeration. Various modern characterization techniques were employed to analyze the properties of the ZnO NPs. A schematic representation of the nanoparticle synthesis process is illustrated in Fig. 2.

2.3.3. Characterization

The synthesized ZnO NPs were characterized to assess their size, shape, elemental composition, and functional properties. The preliminary examination for the formation of ZnO NPs was conducted using a UV–visible spectrophotometer, where the surface plasmon resonance (SPR) was measured. Absorption bands were analyzed with distilled water serving as a reference for baseline correction [31]. FTIR spectroscopy was employed to identify the diverse functionalities of the organic compounds present in the aqueous plant extract, as well as to characterize the metal-oxygen stretching bands within the metal oxide nanoparticles. The FTIR spectra were plotted using Origin Pro 2024 software based on the measured data. XRD was used to confirm the crystallinity of the ZnO NPs, with a wavelength of 1.540 Å at 30 kV. The crystallite size of the ZnO nanoparticles was calculated using the Debye-Scherrer equation using Origin Pro 2024 software.

$$D = \frac{k\lambda}{\beta \cos\theta},$$

where, D = crystallite size of the particles in nm; k = dimensionless and has a value of almost one (0.9); β = FWHM, in radians; λ = wavelength of X-ray (0.15406 nm for Cu Kα); θ = Bragg's angle (in radians).

The different properties such as size, shape, composition, and crystallography were analyzed with the help of FE-SEM images [32]. The grain size of zinc oxide nanoparticles was calculated using Image J software.

2.3.4. Evaluation of antioxidant activity

The free radical scavenging potential of ZnO NPs and an aqueous plant extract was evaluated using the DPPH assay, following established protocols [33,34]. Quercetin, at varying concentrations ranging from 0.62 μg/mL to 20 μg/mL, served as the positive control. For the ZnO NPs, a stock solution was prepared by serial dilution to a final concentration of 15.62 μg/mL from an initial concentration of 250 μg/mL. Similarly, the aqueous plant extract was prepared at a concentration of 15.62 μg/mL from a stock solution of 500 μg/mL. In a 96-well plate, 100 μL of each sample (ZnO NPs and plant extract) was loaded in triplicate, followed by the addition of 100 μL of DPPH solution to each well. The plates were then incubated in the dark for 30 min to allow for reaction and the absorbance was measured at 517 nm. The radical scavenging capacity was calculated using the following formula:

$$\text{Radical scavenging capacity} = \left[\left(\left(A_{control} - A_{sample}\right) / \ A_{control}\right)\right] \times 100$$

where, $A_{control=}$absorbance of control, A_{sample} = absorbance of sample.

2.3.5. Evaluation of antibacterial activity

The antibacterial potential of zinc oxide nanoparticles and an aqueous plant extract were evaluated by the agar well diffusion method [35,36]. The test microorganisms ATCC 25312 *Escherichia coli*, ATCC 700603 *Klebsiella pneumonae*, ATCC 43300 *Staphylococcus aureus*, and ATCC 25931 *Shigella sonnei* were cultured in Mueller Hinton Broth (MHB) and kept in incubation for 24 h at 37 °C in which the turbidity was maintained by matching with 0.5 McFarland. The 50 μg/mL stock solution of ZnO NPs was prepared by dissolving 50 mg of nanoparticles in distilled water from which a test solution was prepared. The 50 μL of ZnO NPs was loaded into each well of Petri dishes. A 50 μg/mL equal volume of neomycin and 50 % DMSO were used as positive and negative controls. After loading the sample, the Petri dishes were left to allow for diffusion and incubated overnight. The zone of inhibition shown by the ZnO NPs against the bacterial strains used was measured. The same protocol was used to evaluate the antibacterial activity shown by the plant extract.

2.3.6. Determination of minimum inhibitory concentration (MIC) and minimum bactericidal concentration (MBC)

The Resazurin microtiter method was adopted to determine the MIC and MBC of zinc oxide nanoparticles [37]. The MHB media was used to grow the bacteria at 37 °C. The turbidity that shows the bacterial growth was checked by using 0.5 McFarland. The 100 μL of double-strength MHB was loaded in each well of 96-well plates. The media column and bacterial column of 96-well plates contain the MHB media. The bacterial suspension was diluted 1/100 times. After that, 10 μL of bacterial suspension was loaded into every well except the well of the media control column. The drug neomycin was used as a control. The 96-well plates were incubated for 18–24 h at 37 °C. Subsequently, 5 μL of a 0.003 % resazurin solution was mixed in each well, and the mixture was incubated for 3 h. After incubation, the colour change was observed. The MIC and MBC shown by the ZnO NPs against the organisms used were determined qualitatively by visual inspection whereas the quantitative determination was performed by using nutrient agar (NA).

2.3.7. Brine shrimp lethality assay (BSLA)

The toxic effect shown by the zinc oxide nanoparticles was tested against Brine shrimp nauplii by adopting the standard protocol suggested by Baravalia et al. [38]. The artificial seawater was prepared and maintained a pH of around 8 to 8.5 by adding 1M NaOH. The ZnO NPs were diluted to various concentrations such as 1000, 800, 500, 250, 125, 100, and 10 μg/mL using stock solution. After that, 4 mL of artificial sea salt water, 500 μL of sample, and 10 nauplii were kept in each test tube in triplicate. Artificial seawater served as the negative control and potassium dichromate solution as the positive control. The dead nauplii were counted after 24 h and the mortality percentage was calculated.

$$\%\ \text{mortality} = \frac{\textit{Number of dead nauplii}}{\textit{Number of total nauplii used}} \times 100$$

By using the Probit value table, the linear equation can be obtained as $Y = mx + c$, where 'Y' is the Probit value at 50 % mortality, 'm' is variable, and 'c' is the intercept. 'x' is the lethal concentration and finally, the lethal concentration (LC_{50}) was calculated.

2.3.8. Statistical analysis

Antioxidant activity was calculated and reported as mean ± standard error. The fifty percent inhibitory concentration (IC_{50}) for each experiment was determined using GraphPad Prism (version 8.0.2.263). Data generated from UV–vis spectroscopy, FTIR spectroscopy, and XRD were analyzed using OriginPro software. FE-SEM images were processed using ImageJ software, and Microsoft Excel (Office 2016) was utilized to construct the graphs.

3. Results and discussion

3.1. UV–vis spectroscopic analysis

The formation of ZnO NPs was preliminarily checked by UV–visible spectroscopy measured in the range of 300–600 nm. The oscillation of the metal nanoparticles caused the free electrons to be in resonance with the light waves. The metal nanoparticles acquire their unique properties by surface plasmon resonance (SPR). The UV–vis absorption band at 361 nm supports the formation of ZnO nanoparticles but the UV–vis absorption band was not seen in an aqueous extract. The UV–visible spectrum of an aqueous extract and ZnO NPs is displayed in Fig. 3.

The SPR of the ZnO NPs is measured by UV–vis spectroscopy [39]. The absorbance was reported at 374 nm in the previously synthesized zinc oxide nanoparticles synthesized using *Deverra tortuosa* [40]. There is no UV–vis absorbance recorded in an aqueous plant extract of *A. nepalensis* D. Don.

3.2. FTIR analysis

Identification of functionalities of the organic compounds present in plant extract and bonding information in ZnO NPs was analyzed by FTIR. The FTIR spectra produced in an aqueous plant extract and synthesized zinc oxide nanoparticles were captured between wavenumber 500-4000 cm^{-1}. Some of the Phytochemicals with ZnO NPs act as a capping and reducing agent to reduce the

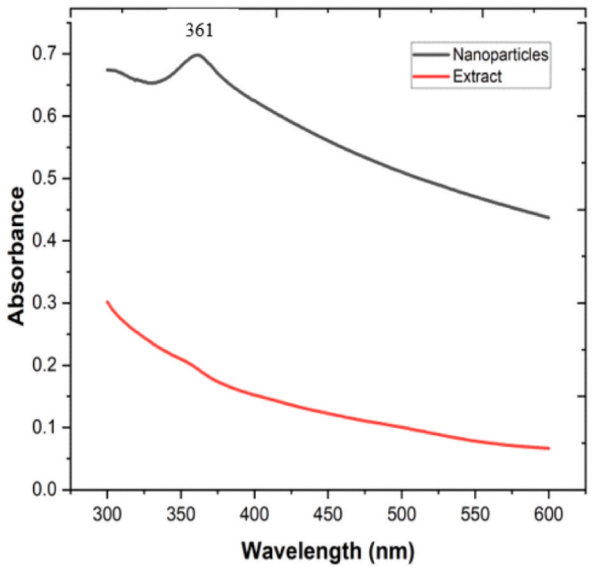

Fig. 3. UV–visible spectral analysis of plant-assisted ZnO NPs and aqueous plant extract.

Zn^{2+} ions. The metal-oxygen stretching absorption range is normally 400-800 cm^{-1} [41]. The FTIR shows the absorption bands at 3317 cm^{-1}, 2971 cm^{-1}, 2897 cm^{-1}, 2158 cm^{-1}, 1592 cm^{-1}, 1383 cm^{-1}, 1249 cm^{-1}, 1044 cm^{-1}, 877 cm^{-1}, and 520 cm^{-1}. The FTIR absorption peaks in an aqueous extract are in 3317 cm^{-1}, 2918 cm^{-1}, 2327 cm^{-1}, 1599 cm^{-1}, 1394 cm^{-1}, 1058 cm^{-1}, and 672 cm^{-1}. The shifting in FTIR band positions and changes in the spectrum patterns give information about the involvement of the organic compounds present in the crude extract to synthesize ZnO nanoparticles. The FTIR spectrum of ZnO NPs and an aqueous plant extract are shown in Fig. 4.

The FTIR spectrum of the ZnO NPs demonstrates significant differences from that of the crude aqueous extract, indicating the involvement of organic compounds from the plant extract in the formation of ZnO nanoparticles. The FTIR spectrum of the aqueous extract reveals strong absorption bands at 3317 cm^{-1}, attributed to the O-H stretching of polyphenolic compounds. In contrast, this peak either disappears or exhibits a marked reduction in the spectrum of ZnO NPs [42]. Additionally, a strong absorption band observed at 2972 cm^{-1} corresponds to C-H stretching. The spectrum further exhibits a narrow and weak peak at 2158 cm^{-1}, indicative of the stretching mode of the -CO group, while the peak at 1383 cm^{-1} corresponds to C-H bending vibrations, and the peak at 1044 cm^{-1} signifies C-O-C vibrations [43]. Strong broadband at 1592 cm^{-1} is associated with the N-O stretching in nitro compounds. Furthermore, the FTIR spectrum of ZnO NPs displays two notable bands at 877 cm^{-1} and 520 cm^{-1}, which arise from the interaction between zinc oxide nanoparticles and various organic moieties present in the aqueous plant extract. The absorption peaks observed in the range of 500–900 cm^{-1} further suggest the successful formation of ZnO NPs [44]. It has been reported that the -OH stretching, -CO stretching, N-O stretching of nitro compounds, C-O-C vibrations, and C-H stretching functionalities are critical for the reduction and capping of Zn^{2+} ions during ZnO NPs formation [45,46]. In plant-assisted synthesis, the donor-acceptor mechanism facilitates the reduction of Zn^{2+} ions, while hydroxyl or oxygen molecules present in the aqueous plant extract oxidize the -OH groups [47]. The FTIR results confirm the presence of plant metabolites associated with ZnO NPs, including flavonoids, alkaloids, carboxylic acids, and polyphenols. These compounds, particularly phenolics and flavonoids, play a crucial role in the reduction of zinc ions to form ZnO NPs [40]. Thus, the FTIR analysis shows the synthesis of ZnO nanoparticles is facilitated by the presence of distinct organic compounds with varying functionalities in the aqueous extract of *A. nepalensis* D. Don.

3.3. X-ray diffraction (XRD)

The X-ray diffraction (XRD) analysis reveals that the ZnO NPs possess a hexagonal wurtzite structure. This is evidenced by the presence of seven prominent peaks at specific 2θ values: 34.47° (100), 31.61° (002), 36.28° (101), 47.33° (102), 56.47° (110), 62.85° (103), and 67.90° (112). These diffraction patterns match with the JCPDS) card number 01-079-0208, confirming the crystalline nature of the material. The average crystallite size of the ZnO NPs was calculated using the Debye-Scherrer formula, yielding a value of 15.31 nm. This result is comparable to previously reported sizes, such as 16.21 nm [48], indicating consistency and reliability in the synthesis and characterization methods. The XRD patterns of ZnO NPs are illustrated in Fig. 5, highlighting the distinct peaks that characterize their crystalline structure.

3.4. Field emission scanning electron microscopy (FE-SEM)

FE-SEM images were employed to examine the grain size and surface features of the ZnO NPs. The images revealed that the nanoparticles have an irregular, quasi-spherical shape with an average grain size of 67.29 nm. This morphology is likely due to the presence of phytochemicals on the surface, which increase surface area, and polarity and promote electrostatic interactions between

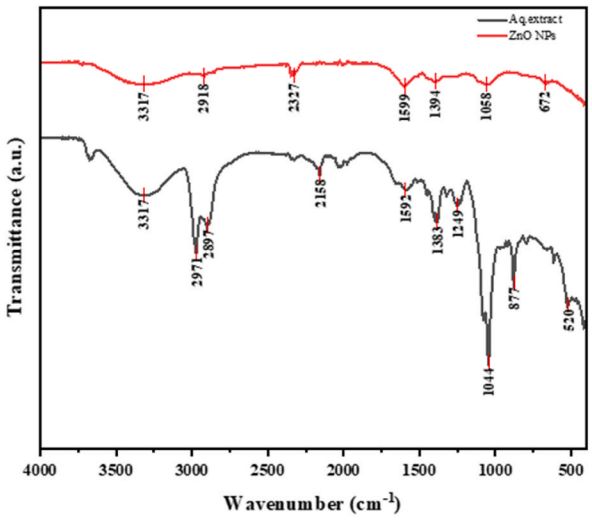

Fig. 4. FTIR spectrum of an aqueous plant extract and synthesized zinc oxide nanoparticles.

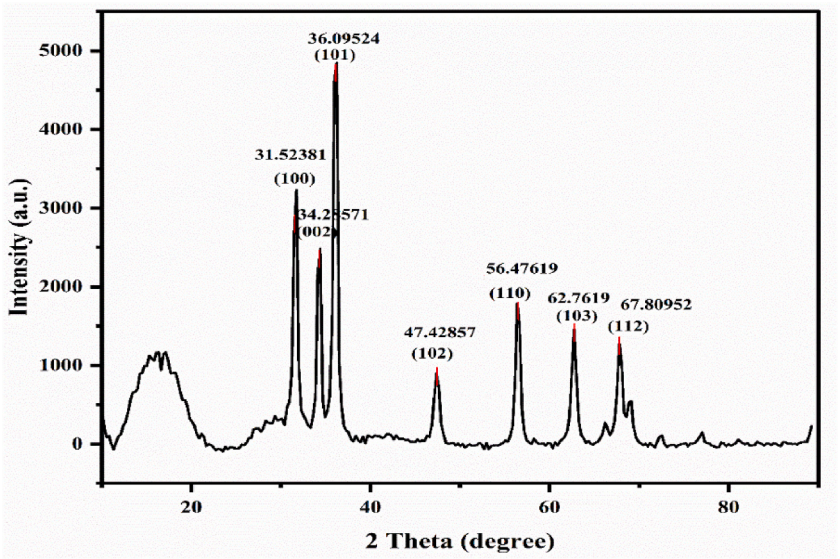

Fig. 5. XRD pattern of plant-assisted synthesized ZnO NPs.

the particles [49–51]. The average grain size of the ZnO NPs was calculated as 67.29 nm, which is almost the same as the size reported by the previous researcher in the study of plant-assisted synthesis of nanoparticles [52]. The FE-SEM images are shown in Fig. 6 (a), (b), and (c).

The percentage of each element in the ZnO NPs was analyzed using EDX spectroscopy. The analysis detected the presence of carbon, nitrogen, nickel, oxygen, and silver in the nanoparticles. The small amount of silver detected is likely due to impurities in the

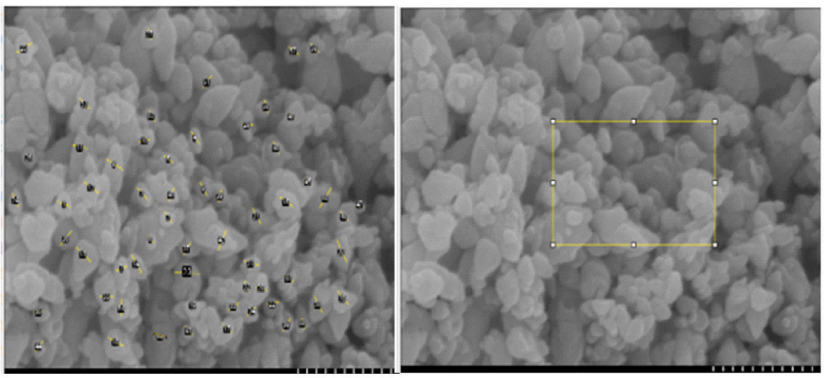

(a) Calculated grain size FE-SEM images at a 500 nm resolution

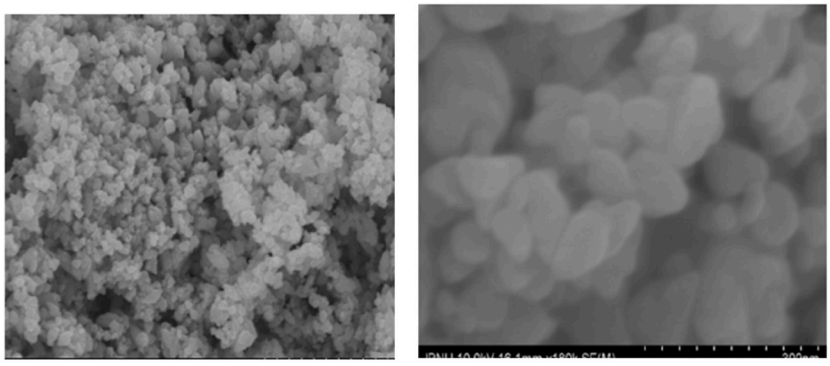

(b) FE-SEM images at a resolution of 2 μm (c) FE-SEM images at a 300 nm resolution

Fig. 6. FE-SEM images of synthesized zinc oxide nanoparticles.

laboratory reagents used during the synthesis process [53,54]. The overall and individual elemental mapping images of the ZnO NPs are shown in Fig. 7. The EDX spectrum, shown in Fig. 8, shows a strong peak at around 1 keV, which is consistent with previous studies on ZnO NPs [55]. The EDX results showed that the ZnO NPs are composed of 66.8 % zinc, 21.3 % oxygen, 9.8 % carbon, 1.9 % nitrogen, and trace amounts of nickel (0.1 %) and silver (0.1 %). These percentages are summarized in Table 1. The dispense of the particles with their size is displayed in the histogram Fig. 9.

3.5. Antioxidant potential

The radical scavenging activity of the crude plant extract and ZnO NPs was assessed by determining the inhibitory concentration (IC_{50}). The IC_{50} of ZnO NPs was found to be 53.02 ± 3.43 μg/mL, whereas the aqueous plant extract showed an IC_{50} of 62.16 ± 3.66 μg/mL. These results indicate that ZnO NPs exhibit a stronger antioxidant activity than the plant extract alone. However, the antioxidant activity of ZnO NPs was less than that of the quercetin, which demonstrated an IC_{50} of 3.43 ± 1.61 μg/mL. This suggests that while ZnO NPs possess significant antioxidant potential their efficacy is less than that of quercetin. A comparison with the already reported results shows that the IC_{50} of zinc oxide nanoparticles synthesized using *C. candelabrum* was reported to be 95.09 μg/mL [56]. In contrast, the ZnO NPs synthesized in this study exhibit enhanced antioxidant activity, as indicated by the lower IC_{50} value. The plots of percentage radical inhibition versus concentration for ZnO NPs (Fig. 10a), the aqueous plant extract (Fig. 10b), and quercetin (Fig. 10c) are presented. The IC_{50} values for the plant-assisted ZnO NPs and the aqueous extract are summarized in Table 2.

The antioxidant potential of nanoparticles is influenced by their size, with smaller ZnO nanoparticles typically exhibiting greater

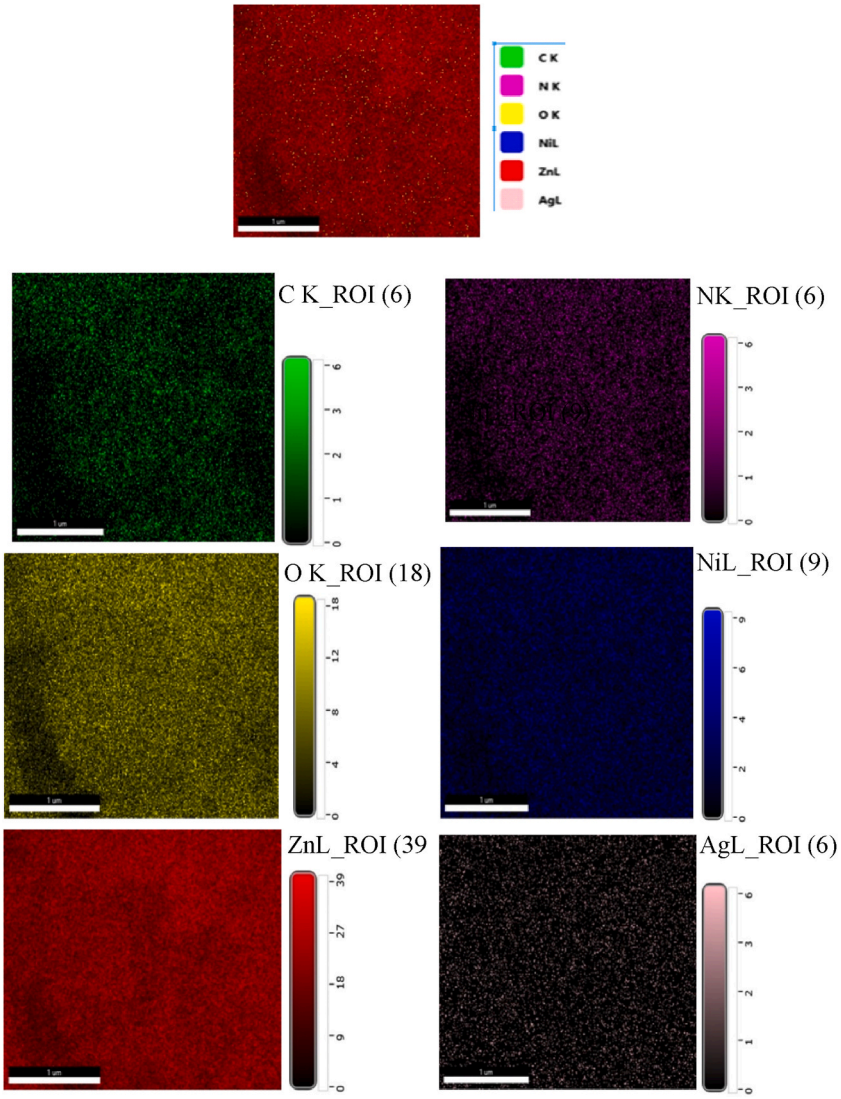

Fig. 7. An energy-dispersive X-ray (EDX) spectrum of ZnO NPs with total and individual colour mapping images.

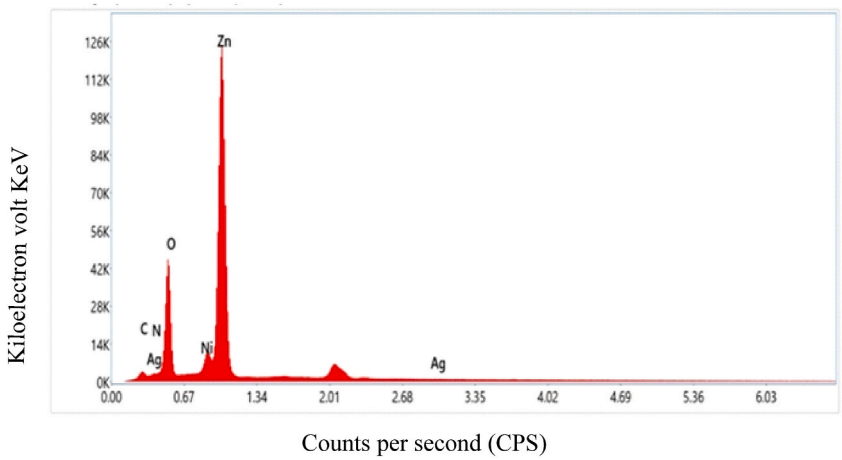

Fig. 8. EDX spectrum of zinc oxide nanoparticles.

Table 1
Composition of synthesized zinc oxide nanoparticles.

Elements	Weight %	Atomic %
C K	9.8	24.8
N K	1.9	4.0
O K	21.3	40.3
Ni L	0.1	0.0
Zn L	66.8	30.9
Ag L	0.1	0.0

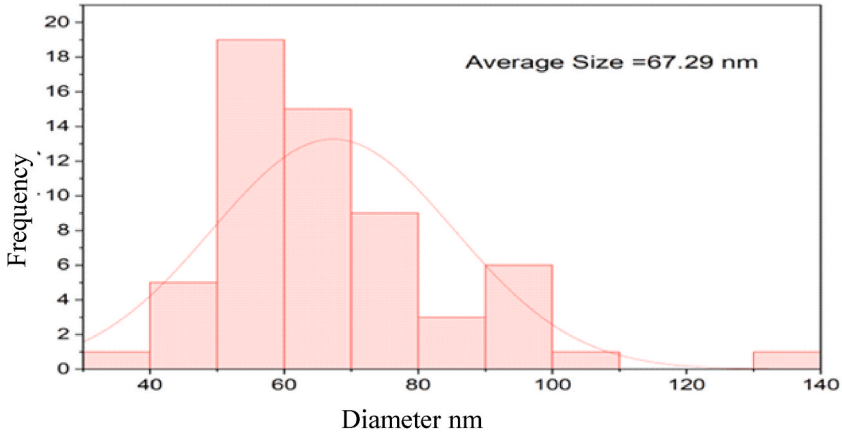

Fig. 9. Size distribution histogram of synthesized zinc oxide nanoparticles.

interaction with DPPH (2,2-diphenyl-1-picrylhydrazyl) reagents. The methanolic solution of DPPH is initially deep violet and unstable, but upon interaction with ZnO NPs, electrons are migrated from the oxygen atom of the zinc oxide nanoparticles to the unpaired electron of the nitrogen atom in the DPPH molecule. This electron transfer leads to the reduction of DPPH, resulting in the formation of a DPPH molecule with a light-yellow color, as shown in Fig. 11 [57]. The charge density on the surface of the synthesized ZnO NPs, which is influenced by the biological cell components that capped the nanoparticles, further enhances their interaction with DPPH molecules. Consequently, the plant-assisted synthesis of ZnO NPs exhibited potent antioxidant activity [58]. In this process, DPPH is reduced by the transfer of electrons or hydrogen atoms from the antioxidant, demonstrating the effective scavenging ability of the ZnO NPs.

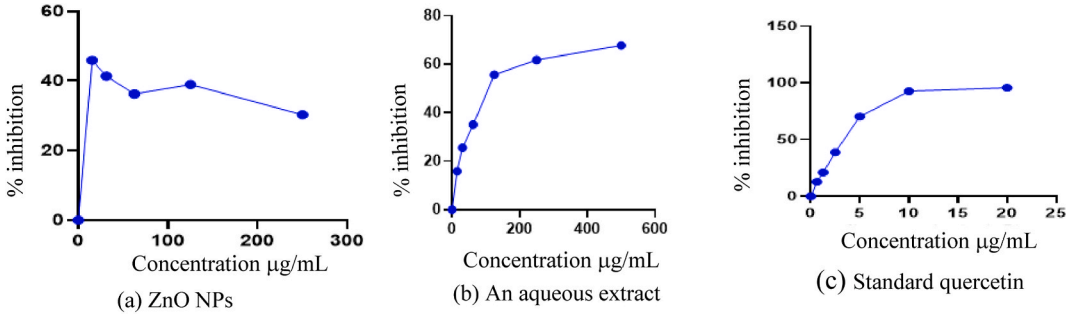

Fig. 10. A plot of percentage radical inhibition against the concentration of (a) ZnO NPs (b) Aqueous extract and (c) Standard quercetin.

Table 2
Antioxidant potential (IC_{50}) shown by zinc oxide nanoparticles, aqueous extract and standard.

Part used	Nanoparticles	IC_{50} (µg/mL)
Bark	ZnO NPs	53.02 ± 3.43
	Aqueous	62.16 ± 3.66
	[a]Quercetin	3.43 ± 1.61

[a] Note: Quercetin = positive control.

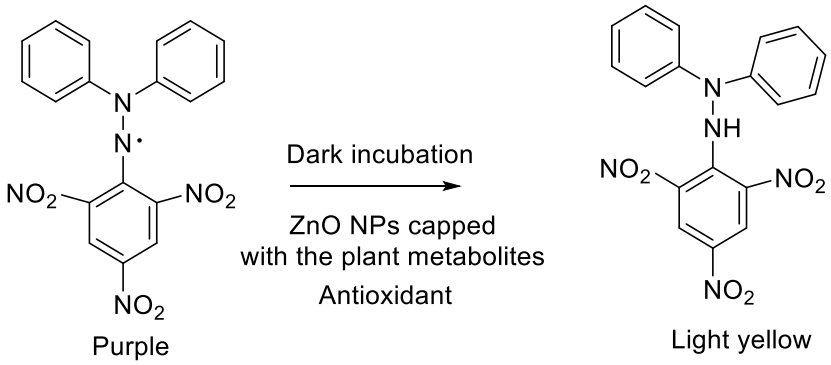

Fig. 11. Mechanism of antioxidant activity shown by ZnO NPs capped with the plant metabolites.

3.6. Antimicrobial activity

The antimicrobial potential shown by the zinc oxide nanoparticles and an aqueous plant extract against the different bacterial strains is displayed in Table 3.

The ZOI shown by ZnO NPs was 18 mm against *K. pneumoniae* and *E. coli.*, which was closer to the ZOI shown by the positive control neomycin, 28 mm against *K. pneumoniae,* and 23 mm against *E. coli*. The aqueous plant extract showed a ZOI of 12 mm against *E. coli* which was found less active (ZOI of 23 mm) as compared to the positive control (ZOI of 23 mm). Fig. 12 and 13A-D show the results of antibacterial activity by an aqueous plant extract and ZnO NPs.

Zinc oxide nanoparticles exhibit potential antibacterial action by stimulating multiple bactericidal mechanisms, including the production of reactive oxygen species (ROS) such as hydroxyl radicals ($OH^{\cdot}$) and peroxide, as well as the release of Zn^{2+} ions. These mechanisms result in oxidative stress, disruption of bacterial cell membranes, and damage to bacterial DNA, ultimately causing cell death [59–61]. The dissolution of ZnO NPs releases Zn^{2+} ions, which interact with bacterial cell membranes and organelles, causing damage and leakage of intracellular components [62]. Additionally, superoxide radicals ($\bullet O^{-2}$) are generated, leading to the formation of hydrogen peroxide (H_2O_2), which penetrates bacterial cells and damages organelles, contributing to cell death [63]. The amount of hydrogen peroxide produced is directly proportional to the size of the ZnO NPs, further enhancing their bactericidal properties [64, 65]. The ZnO NPs also adhere to the surface of dead bacteria, continuing to produce ROS and preventing bacterial growth [66]. These unique physiochemical characteristics, particularly the high exposed surface area of ZnO NPs, make them highly effective antibacterial agents against antibiotic-resistant bacteria. Fig. 14 demonstrates the antimicrobial mechanisms of plant-mediated synthesized nanoparticles.

Table 3
ZOI shown by ZnO NPs and an aqueous extract.

Plant Part	Plant extracts	Bacteria	ZOI of the sample (mm)	ZOI of positive control neomycin (mm)
Bark	ZnO NPs	*Klebsiella pneumoniae*	18	28
		Escherichia coli	18	23
		Shigella sonnei	16	28
		Staphylococcus aureus	12	23
	Aqueous	*Klebsiella pneumoniae*	10	28
		Escherichia coli	12	23
		Shigella sonnei	11	28
		Staphylococcus aureus	9	23

*ZOI = Zone of inhibition.

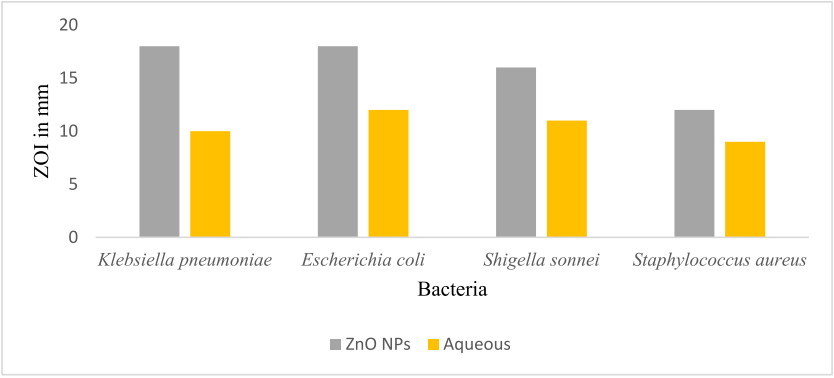

Fig. 12. Antibacterial activity shown (ZOI in mm) by synthesized zinc oxide nanoparticles and aqueous extract against *K. pneumoniae*, *E. coli*, *S. sonnei,* and *S. aureus*.

3.7. MIC and MBC

The MIC and MBC of ZnO NPs against *Klebsiella pneumoniae* were found to be 0.39 mg/mL and 0.78 mg/mL, respectively Fig. 15(A, B). Against *Staphylococcus aureus*, the MIC and MBC were 0.78 mg/mL and 1.56 mg/mL, respectively. In comparison, the positive control showed a much lower MIC of 0.007 mg/mL and an MBC of 0.015 mg/mL for both bacterial strains. The results of the MIC and MBC shown by ZnO NPs are presented in Table 4.

The change in color of resazurin dye helps differentiate between live and dead cells in a mixture. Live cells reduce resazurin's purple color to pink by converting it into resorufin, a process facilitated by mitochondrial NADH enzymes [67]. This color change mechanism in living cells is illustrated in Fig. 16.

3.8. Toxicity analysis

The lethal concentration (LC) of ZnO nanoparticles (ZnO NPs) against brine shrimp nauplii was found to be 16.59 μg/mL. In the positive control using $K_2Cr_2O_7$, all nauplii died, while an equal number of nauplii survived in the negative control using 50 % DMSO. The dead nauplii and the percentage of mortality following nanoparticle treatment are shown in Table 5, and the LC_{50} of ZnO NPs is shown in Table 6. A probit plot against Log C (concentration) is displayed in Fig. 17.

The nanoparticles have large exposed surface areas due to which they have the potential to cause significant harm to the human body and the environment. To mitigate these harmful effects, several methods have been developed to detoxify metal and metal oxide nanoparticles. One such method involves treating the synthesized nanoparticles with carbon, which reduces the metal oxides to free metals. This process applies to oxides of metals like zinc (Zn), iron (Fe), nickel (Ni), tin (Sn), and lead (Pb), which are reduced by heating with carbon. In practice, metal oxides are mixed with coke, a carbon source, and heated in a furnace where carbon reacts with oxygen to release the free metal [68]. At low concentrations, however, ZnO NPs are considered nontoxic.

4. Conclusion

The synthesis of zinc oxide nanoparticles using plant extracts is a rapid, economical, environmentally friendly, and efficient method. In this study, the aqueous extract of *A. nepalensis* D. Don was utilized to synthesize zinc oxide nanoparticles (ZnO NPs) for various biological applications. The formation of ZnO NPs was confirmed using UV–visible spectroscopy by measuring SPR. The aqueous plant extracts contain a diverse array of organic compounds with different functional groups, which act as capping, stabilizing, and reducing agents during the formation of ZnO NPs. The range of metal-oxygen interactions in ZnO NPs can be identified by

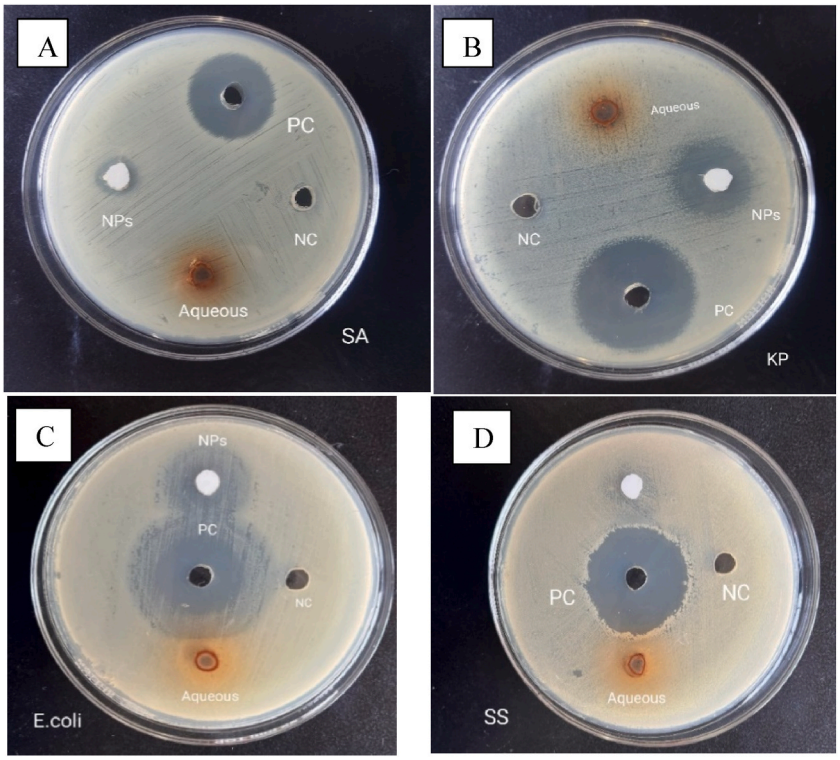

SA= Staphylococcus aureus, KP = Klebsiella pneumoniae
E. coli = Escherichia coli, SS = S. sonnei

Fig. 13. Antibacterial activity shown by ZnO NPs and an aqueous plant extract against (A) *S. aureus*, (B) *K. pneumoniae* (C) *E. coli,* and (D) *Shigella. sonnei.*

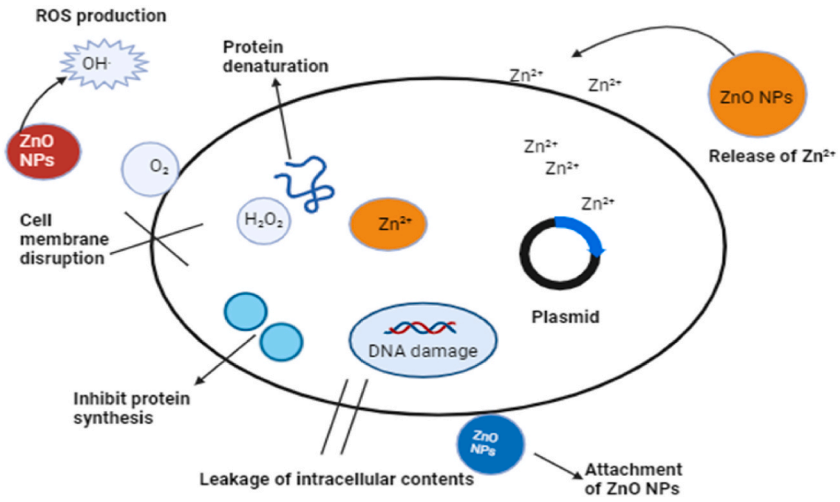

Fig. 14. Mechanism of antibacterial property shown by the ZnO NPs.

peaks appearing in the 500–900 cm^{-1} in FTIR. XRD analysis can be used to determine the crystallite size of the ZnO NPs, FE-SEM provides insights into grain size and surface morphology. EDX color mapping images reveal the composition of different elements of the nanoparticles. Additionally, the ZnO NPs synthesized using plant extracts exhibited high antioxidant capacity by scavenging DPPH radicals. The nanoparticles show good antibacterial activity against various bacteria, indicating their potential as alternative antibacterial drug candidates in future drug design processes. The wide range of biological applications of ZnO NPs supports their

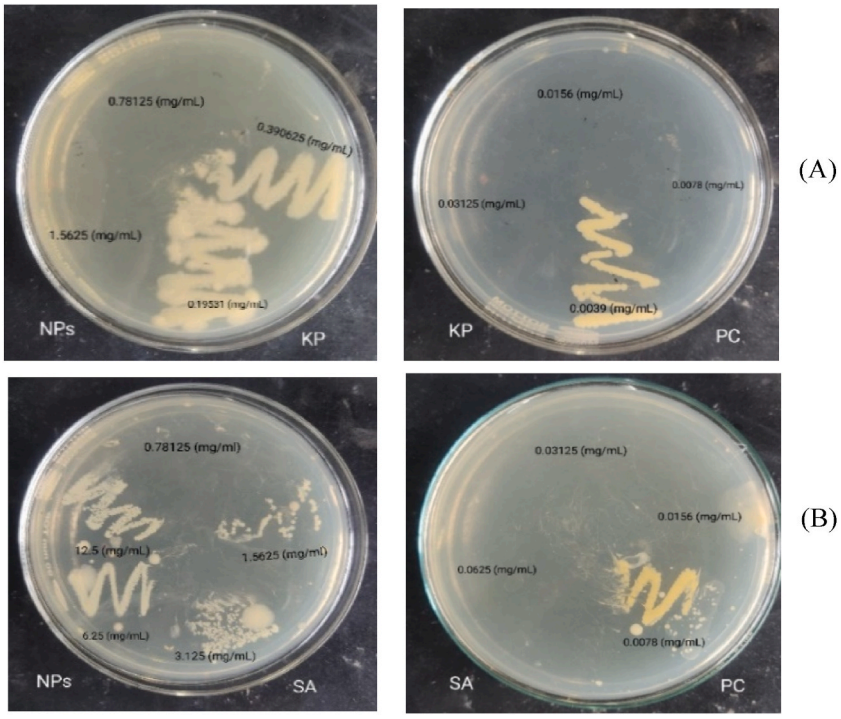

Fig. 15. MIC and MBC of ZnO NPs against (A) *K. pneumoniae* and (B) *Staphylococcus aureus*.

Table 4
MIC and MBC of ZnO NPs against *K. pneumoniae* and *S. aureus*.

Nanoparticles	*Klebsiella pneumoniae*		*Staphylococcus aureus*	
	MIC (mg/mL)	MBC (mg/mL)	MIC (mg/mL)	MBC (mg/mL)
ZnO NPs	0.39	0.78	0.78	1.56
Positive control	0.003	0.007	0.007	0.015

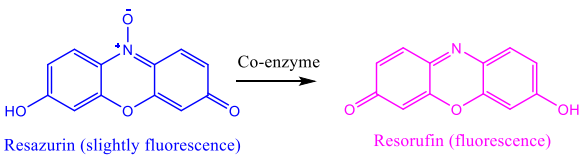

Fig. 16. Showing reduction of resazurin by co-enzymes in living bacterial cells showing MIC and MBC.

Table 5
The number of dead nauplii after treatment with zinc oxide nanoparticles and the percentage mortality.

Nanoparticles	Concentration (μg/mL)	Total no. of dead nauplii	% mortality
ZnO NPs	10	16	53.33
	100	17	56.66
	125	20	66.66
	250	17	56.66
	500	22	73.33
	800	23	76.66
	1000	26	86.66

potential in developing new medications. Further research is strongly recommended for the extraction, isolation, and characterization of active plant metabolites from this plant sample, as they may serve as precursors in the formation of ZnO NPs and contribute to future drug development efforts.

Table 6
LC_{50} of synthesized ZnO NPs against brine shrimp nauplii.

Synthesized ZnO nanoparticles	Linear equation	LC_{50} (μg/mL)
ZnO NPs	5.00 = 0.426x + 4.4761	16.59

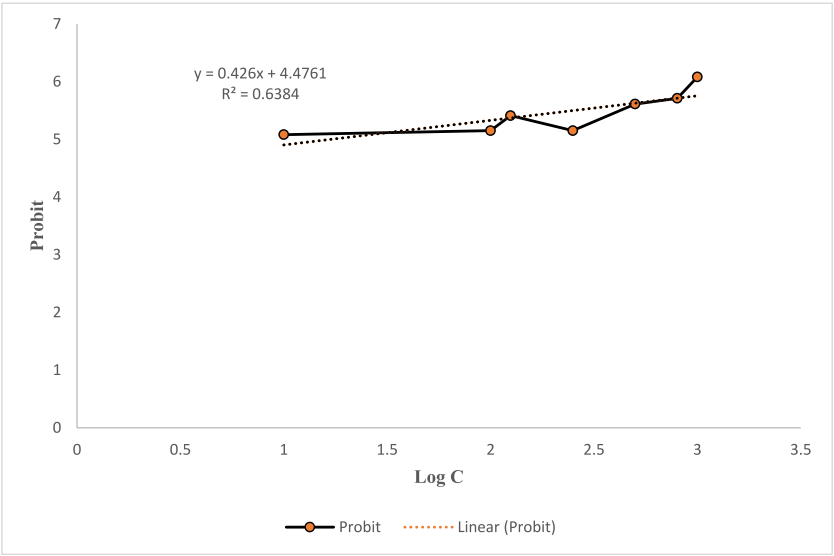

Fig. 17. A plot showing probit against Log C.

CRediT authorship contribution statement

Dipak Raj Jaishi: Data curation. **Indra Ojha:** Data curation. **Govinda Bhattarai:** Data curation. **Rabina Baraili:** Data curation. **Ishwor Pathak:** Data curation. **Dinesh Raj Ojha:** Data curation. **Deepak Kumar Shrestha:** Data curation. **Khaga Raj Sharma:** Formal analysis, Data curation, Conceptualization.

Additional information

For this work, no further information is provided.

Data availability statement

All of the data produced in this research will be provided if requested.

Funding statement

Financial funding for this research was provided by the University Grants Commission (UGC), Nepal (Award No. CRIG-78/79-S and T-01).

Declaration of competing interest

The authors declare the following financial interests/personal relationships which may be considered as potential competing interests:Khaga Raj Sharma reports financial support was provided by University Grants Commission. Khaga raj Sharma reports a relationship with University Grants Commission that includes: funding grants. Khaga Raj Sharma has patent Not pending to Not. Not any financial support from other institutions support If there are other authors, they declare that they have no known competing financial interests or personal relationships that could have appeared to influence the work reported in this paper.

Acknowledgments

The authors would like to express their gratitude to the National Herbarium and Plant Laboratories in Godawari, Lalitpur, Nepal, for assisting in the identification of the plant. We also thank the Nepal Academy of Science and Technology (NAST), Lalitpur, Nepal, for

providing the XRD data. Our appreciation extends to the Institute of Biomolecule Reconstruction at Sun Moon University, Republic of Korea, for supplying the bacterial strains. We are thankful to the University Grants Commission of Nepal for their financial support. Special thanks are due to Prof. Dr. Niranjan Parajuli, the Principal Investigator of the project, for his invaluable support throughout this research.

References

[1] C. Xia, W. Zhao, J. Wang, J. Sun, G. Cui, L. Zhang, Progress on geographical distribution, driving factors and ecological functions of Nepalese alder, Diversity 15 (1) (2023) 59, https://doi.org/10.3390/d15010059.
[2] S.C. Sati, N. Sati, O.P. Sati, Bioactive constituents and medicinal importance of genus Alnus, Pharmacogn. Rev 5 (10) (2011) 174–183, https://doi.org/10.4103/0973-7847.91115.
[3] S. Laurent, D. Forge, M. Port, A. Roch, C. Robic, L. Vander Elst, R.N. Muller, Magnetic iron oxide nanoparticles: synthesis, stabilization, vectorization, physicochemical characterizations, and biological applications, Chem. Rev. 108 (6) (2008) 2064–2110, https://doi.org/10.1021/cr068445e.
[4] M. Nadeem, D. Tungmunnithum, C. Hano, B.H. Abbasi, S.S. Hashmi, W. Ahmad, A. Zahir, The current trends in the green syntheses of titanium oxide nanoparticles and their applications, Green Chem. Lett. Rev. 11 (4) (2018) 492–502, https://doi.org/10.1080/17518253.2018.1538430.
[5] R. Gul, H. Jan, G. Lalay, A. Andleeb, H. Usman, R. Zainab, Z. Qamar, C. Hano, B.H. Abbasi, Medicinal plants and biogenic metal oxide nanoparticles: a paradigm shift to treat Alzheimer's disease, Coatings 11 (6) (2021) 717, https://doi.org/10.3390/coatings11060717.
[6] S. Jadoun, R. Arif, N.K. Jangid, R.K. Meena, Green synthesis of nanoparticles using plant extracts: a review, Environ. Chem. Lett. 19 (1) (2021) 355–374, https://doi.org/10.1007/s10311-020-01074-x.
[7] Sumaira, T. Khan, B. Haider Abbasi, M. Siddique Afridi, F. Tanveer, I. Ullah, S. Bashir, C. Hano, Melatonin-enhanced biosynthesis of antimicrobial AgNPs by improving the phytochemical reducing potential of a callus culture of Ocimum basilicum L. Var. Thyrsiflora, RSC Adv. 7 (61) (2017) 38699–38713, https://doi.org/10.1039/C7RA05044E.
[8] H. Jan, M. Shah, H. Usman, M.A. Khan, M. Zia, C. Hano, B.H. Abbasi, Biogenic synthesis and characterization of antimicrobial and antiparasitic zinc oxide (ZnO) nanoparticles using aqueous extracts of the Himalayan Columbine (Aquilegia pubiflora), Front. Mater. 7 (2020), https://doi.org/10.3389/fmats.2020.00249.
[9] M. Shah, S. Nawaz, H. Jan, N. Uddin, A. Ali, S. Anjum, N. Giglioli-Guivarc'h, C. Hano, B.H. Abbasi, Synthesis of bio-mediated silver nanoparticles from *Silybum marianum* and their biological and clinical activities, Mater. Sci. Eng. C 112 (2020) 110889, https://doi.org/10.1016/j.msec.2020.110889.
[10] M. Sundrarajan, S. Ambika, K. Bharathi, Plant-extract mediated synthesis of ZnO nanoparticles using *Pongamia pinnata* and their activity against pathogenic bacteria, Adv. Powder Technol. 26 (5) (2015) 1294–1299, https://doi.org/10.1016/j.apt.2015.07.001.
[11] T. Mustapha, N. Misni, N.R. Ithnin, A.M. Daskum, N.Z. Unyah, A review on plants and microorganisms mediated synthesis of silver nanoparticles, role of plants metabolites and applications, Int. J. Environ. Res. Publ. Health 19 (2) (2022) 674, https://doi.org/10.3390/ijerph19020674.
[12] J. Jeevanandam, S.F. Kiew, S. Boakye-Ansah, S.Y. Lau, A. Barhoum, M.K. Danquah, J. Rodrigues, Green approaches for the synthesis of metal and metal oxide nanoparticles using microbial and plant extracts, Nanoscale 14 (7) (2022) 2534–2571, https://doi.org/10.1039/d1nr08144f.
[13] I. Ijaz, E. Gilani, A. Nazir, A. Bukhari, Detail review on chemical, physical and green synthesis, classification, characterizations and applications of nanoparticles, Green Chem. Lett. Rev. 13 (3) (2020) 223–245, https://doi.org/10.1080/17518253.2020.1802517.
[14] J. Jiang, J. Pi, J. Cai, The advancing of zinc oxide nanoparticles for biomedical applications, Bioinorgan. Chem. Appl. 2018 (2018) 1062562, https://doi.org/10.1155/2018/1062562.
[15] R. Al-Shalabi, R. Abu-Huwaij, R. Hamed, M.M. Abbas, The antimicrobial and the antiproliferative effect of human triple negative breast cancer cells using the greenly synthesized iron oxide nanoparticles, J. Drug Deliv. Sci. Technol. 75 (2022) 103642, https://doi.org/10.1016/j.jddst.2022.103642.
[16] M. Murali, N. Kalegowda, H.G. Gowtham, M.A. Ansari, M.N. Alomary, S. Alghamdi, N. Shilpa, S.B. Singh, M.C. Thriveni, M. Aiyaz, N. Angaswamy, N. Lakshmidevi, S.F. Adil, M.R. Hatshan, K.N. Amruthesh, Plant-mediated zinc oxide nanoparticles: advances in the new millennium towards understanding their therapeutic role in biomedical applications, Pharmaceutics 13 (10) (2021) 1662, https://doi.org/10.3390/pharmaceutics13101662.
[17] M. Alhujaily, S. Albukhaty, M. Yusuf, M.K.A. Mohammed, G.M. Sulaiman, H. Al-Karagoly, A.A. Alyamani, J. Albaqami, F.A. AlMalki, Recent advances in plant-mediated zinc oxide nanoparticles with their significant biomedical properties, Bioeng. Basel Switz. 9 (10) (2022) 541, https://doi.org/10.3390/bioengineering9100541.
[18] H.U.R. Bajwa, M.K. Khan, Z. Abbas, R. Riaz, T.U. Rehman, R.Z. Abbas, M.T. Aleem, A. Abbas, M.M. Almutairi, F.A. Alshammari, Y. Alraey, A. Alouffi, Nanoparticles: synthesis and their role as potential drug candidates for the treatment of parasitic diseases, Life Basel Switz 12 (5) (2022) 750, https://doi.org/10.3390/life12050750.
[19] J.B. Baxter, E.S. Aydil, Nanowire-based dye-sensitized solar cells, Appl. Phys. Lett. 86 (5) (2005) 053114, https://doi.org/10.1063/1.1861510.
[20] S.-J. Choi, M. Baek, H.-E. Chung, J. Yu, J.-A. Lee, T.-H. Kim, J.-M. Oh, W.-J. Lee, S.-M. Paek, J.K. Lee, J. Jeong, J.-H. Choy, Pharmacokinetics, tissue distribution, and excretion of zinc oxide nanoparticles, Int. J. Nanomed. 3081 (2012), https://doi.org/10.2147/IJN.S32593.
[21] T.A. Abdel−Baset, M. Belhaj, Structural characterization, dielectric properties and electrical conductivity of ZnO nanoparticles synthesized by Co-precipitation route, Phys. B Condens. Matter 616 (2021) 413130, https://doi.org/10.1016/j.physb.2021.413130.
[22] A. Hatamie, A. Khan, M. Golabi, A.P.F. Turner, V. Beni, W.C. Mak, A. Sadollahkhani, H. Alnoor, B. Zargar, S. Bano, O. Nur, M. Willander, Zinc oxide nanostructure-modified textile and its application to biosensing, photocatalysis, and as antibacterial material, Langmuir ACS J. Surf. Colloids 31 (39) (2015) 10913–10921, https://doi.org/10.1021/acs.langmuir.5b02341.
[23] Z.L. Wang, Functional oxide nanobelts: materials, properties and potential applications in nanosystems and biotechnology, Annu. Rev. Phys. Chem. 55 (2004) 159–196, https://doi.org/10.1146/annurev.physchem.55.091602.094416.
[24] H.B. Ahmed, M.K. Zahran, H.E. Emam, Heatless synthesis of well dispersible Au nanoparticles using pectin biopolymer, Int. J. Biol. Macromol. 91 (2016) 208–219, https://doi.org/10.1016/j.ijbiomac.2016.05.060.
[25] M. Arumugam, D.B. Manikandan, E. Dhandapani, A. Sridhar, K. Balakrishnan, M. Markandan, T. Ramasamy, Green synthesis of zinc oxide nanoparticles (ZnO NPs) using *Syzygium cumini*: potential multifaceted applications on antioxidants, cytotoxic and as nanonutrient for the growth of *Sesamum indicum*, Environ. Technol. Innov. 23 (2021) 101653, https://doi.org/10.1016/j.eti.2021.101653.
[26] A. Fouda, E. Saied, A.M. Eid, F. Kouadri, A.M. Alemam, M.F. Hamza, M. Alharbi, A. Elkelish, S.E.-D. Hassan, Green synthesis of zinc oxide nanoparticles using an aqueous extract of *Punica granatum* for antimicrobial and catalytic activity, J. Funct. Biomater. 14 (4) (2023) 205, https://doi.org/10.3390/jfb14040205.
[27] T.S. Aldeen, H.E. Ahmed Mohamed, M. Maaza, ZnO nanoparticles prepared via a green synthesis approach: physical properties, photocatalytic and antibacterial activity, J. Phys. Chem. Solid. 160 (2022) 110313, https://doi.org/10.1016/j.jpcs.2021.110313.
[28] J. Jalab, W. Abdelwahed, A. Kitaz, R. Al-Kayali, Green synthesis of silver nanoparticles using aqueous extract of Acacia Cyanophylla and its antibacterial activity, Heliyon 7 (9) (2021) e08033, https://doi.org/10.1016/j.heliyon.2021.e08033.
[29] T.U. Doan Thi, T.T. Nguyen, Y.D. Thi, K.H. Ta Thi, B.T. Phan, K.N. Pham, Green synthesis of ZnO nanoparticles using Orange fruit peel extract for antibacterial activities, RSC Adv. 10 (40) (2020) 23899–23907, https://doi.org/10.1039/d0ra04926c.
[30] M.F. Islam, S. Islam, M.A.S. Miah, A.K.O. Huq, A.K. Saha, Z.J. Mou, M.M.H. Mondol, M.N.I. Bhuiyan, Green synthesis of zinc oxide nano particles using Allium cepa L. Waste peel extracts and its antioxidant and antibacterial activities, Heliyon 10 (3) (2024) e25430, https://doi.org/10.1016/j.heliyon.2024.e25430.
[31] K. Anandalakshmi, J. Venugobal, V. Ramasamy, Characterization of silver nanoparticles by green synthesis method using Pedalium murex leaf extract and their antibacterial activity, Appl. Nanosci. 6 (3) (2016) 399–408, https://doi.org/10.1007/s13204-015-0449-z.
[32] X.-F. Zhang, Z.-G. Liu, W. Shen, S. Gurunathan, Silver nanoparticles: synthesis, characterization, properties, applications, and therapeutic approaches, Int. J. Mol. Sci. 17 (9) (2016) 1534, https://doi.org/10.3390/ijms17091534.

[33] T.H.A. Alabri, A.H.S. Al Musalami, M.A. Hossain, A.M. Weli, Q. Al-Riyami, Comparative study of phytochemical screening, antioxidant and antimicrobial capacities of fresh and dry leaves crude plant extracts of *Datura metel* L, J. King Saud Univ. Sci. 26 (3) (2014) 237–243, https://doi.org/10.1016/j.jksus.2013.07.002.

[34] Lie-Fen Shyur, Jieh-Hen Tsung, Je-Hsin Chen, Chih-Yang Chiu, Chiu-Ping Lo, Antioxidant properties of extracts from medicinal plants popularly used in Taiwan, Int. J. Appl. Sci. Eng. 3 (3) (2005) 195–202.

[35] M. Balouiri, M. Sadiki, S.K. Ibnsouda, Methods for in vitro evaluating antimicrobial activity: a review, J. Pharm. Anal. 6 (2) (2016) 71–79.

[36] T.C. Abbey, E. Deak, What's new from the CLSI subcommittee on antimicrobial susceptibility testing M100, in: Clin. Microbiol. Newsl., 29th Edition., 2019, pp. 203–209, https://doi.org/10.1016/j.clinmicnews.2019.11.002, 41 (23).

[37] S.D. Sarker, L. Nahar, Y. Kumarasamy, Microtitre Plate-based antibacterial assay incorporating resazurin as an indicator of cell growth, and its application in the *in vitro* antibacterial screening of phytochemicals, Methods 42 (4) (2007) 321–324, https://doi.org/10.1016/j.ymeth.2007.01.006.

[38] Y. Baravalia, Y. Vaghasiya, S. Chanda, Brine shrimp cytotoxicity, anti-inflammatory and analgesic properties of *Woodfordia fruticosa* Kurz flowers, Iran. J. Pharm. Res. IJPR 11 (3) (2012) 851–861.

[39] C. Rhodes, S. Franzen, J.-P. Maria, M. Losego, D.N. Leonard, B. Laughlin, G. Duscher, S. Weibel, Surface plasmon resonance in conducting metal oxides, J. Appl. Phys. 100 (5) (2006) 054905, https://doi.org/10.1063/1.2222070.

[40] Y.A. Selim, M.A. Azb, I. Ragab, M. H. M. Abd El-Azim, Green synthesis of zinc oxide nanoparticles using aqueous extract of *Deverra tortuosa* and their cytotoxic activities, Sci. Rep. 10 (1) (2020) 3445, https://doi.org/10.1038/s41598-020-60541-1.

[41] R. Gomathi, H. Suhana, Green synthesis, characterization and antimicrobial activity of zinc oxide nanoparticles using *Artemisia pallens* plant extract, Inorg. Nano-Met. Chem. 51 (12) (2021) 1663–1672, https://doi.org/10.1080/24701556.2020.1852256.

[42] A. Hussain, A. Mehmood, G. Murtaza, K.S. Ahmad, A. Ulfat, M.F. Khan, T.S. Ullah, Environmentally benevolent synthesis and characterization of silver nanoparticles using *Olea ferruginea* Royle for antibacterial and antioxidant activities, Green Process. Synth. 9 (1) (2020) 451–461, https://doi.org/10.1515/gps-2020-0047.

[43] J. Depciuch, I. Kasprzyk, E. Roga, M. Parlinska-Wojtan, Analysis of morphological and molecular composition changes in allergenic *Artemisia vulgaris* L. Pollen under traffic pollution using SEM and FTIR spectroscopy, Environ. Sci. Pollut. Res. 23 (22) (2016) 23203–23214, https://doi.org/10.1007/s11356-016-7554-8.

[44] G. Sharmila, M. Thirumarimurugan, C. Muthukumaran, Green synthesis of ZnO nanoparticles using *Tecoma castanifolia* leaf extract: characterization and evaluation of its antioxidant, bactericidal and anticancer activities, Microchem. J. 145 (2019) 578–587, https://doi.org/10.1016/j.microc.2018.11.022.

[45] M. Ihsan, I.U. Din, K. Alam, I. Munir, H.I. Mohamed, F. Khan, Green fabrication, characterization of zinc oxide nanoparticles using plant extract of *Momordica charantia* and *Curcuma zedoaria* and their antibacterial and antioxidant activities, Appl. Biochem. Biotechnol. 195 (6) (2023) 3546–3565, https://doi.org/10.1007/s12010-022-04309-5.

[46] G. Sangeetha, S. Rajeshwari, R. Venckatesh, Green synthesis of zinc oxide nanoparticles by *Aloe barbadensis Miller* leaf extract: structure and optical properties, Mater. Res. Bull. 46 (12) (2011) 2560–2566, https://doi.org/10.1016/j.materresbull.2011.07.046.

[47] S. Alamdari, M. Sasani Ghamsari, C. Lee, W. Han, H.-H. Park, M.J. Tafreshi, H. Afarideh, M.H.M. Ara, Preparation and characterization of zinc oxide nanoparticles using leaf extract of *Sambucus ebulus*, Appl. Sci. 10 (10) (2020) 3620, https://doi.org/10.3390/app10103620.

[48] S. Talam, S.R. Karumuri, N. Gunnam, Synthesis, characterization, and spectroscopic properties of ZnO nanoparticles, Int. Sch. Res. Notices 2012 (1) (2012) 372505, https://doi.org/10.5402/2012/372505.

[49] A. Sajjad, S.H. Bhatti, Z. Ali, G.H. Jaffari, N.A. Khan, Z.F. Rizvi, M. Zia, Photoinduced fabrication of zinc oxide nanoparticles: transformation of morphological and biological response on light irradiance, ACS Omega 6 (17) (2021) 11783–11793, https://doi.org/10.1021/acsomega.1c01512.

[50] M. Bandeira, M. Giovanela, M. Roesch-Ely, D.M. Devine, J. da Silva Crespo, Green synthesis of zinc oxide nanoparticles: a review of the synthesis methodology and mechanism of formation, Sustain. Chem. Pharm. 15 (2020) 100223, https://doi.org/10.1016/j.scp.2020.100223.

[51] Chandrasekar, L. P.; Sethuraman, B. D.; Subramani, M.; Mohandos, S. Green Synthesised ZnO Nanoparticles from Plectranthus Amboinicus Plant Extract: Removal of Safranin- O and Malachite Green Dyes & Anti-Bacterial Activity. Int. J. Environ. Anal. Chem. 0 (0) 1–18. https://doi.org/10.1080/03067319.2023.2190458.

[52] S.S. Rad, A.M. Sani, S. Mohseni, Biosynthesis, characterization and antimicrobial activities of zinc oxide nanoparticles from leaf extract of *Mentha pulegium* (L.), Microb. Pathog. 131 (2019) 239–245, https://doi.org/10.1016/j.micpath.2019.04.022.

[53] M. Ramesh, M. Anbuvannan, G. Viruthagiri, Green synthesis of ZnO nanoparticles using Solanum nigrum leaf extract and their antibacterial activity, Spectrochim. Acta. A. Mol. Biomol. Spectrosc. 136 (2015) 864–870.

[54] H.R. Rajabi, R. Naghiha, M. Kheirizadeh, H. Sadatfaraji, A. Mirzaei, Z.M. Alvand, Microwave assisted extraction as an efficient approach for biosynthesis of zinc oxide nanoparticles: synthesis, characterization, and biological properties, Mater. Sci. Eng. C 78 (2017) 1109–1118, https://doi.org/10.1016/j.msec.2017.03.090.

[55] H. Hameed, A. Waheed, M.S. Sharif, M. Saleem, A. Afreen, M. Tariq, A. Kamal, W.A. Al-onazi, D.A. Al Farraj, S. Ahmad, R.M. Mahmoud, Green synthesis of zinc oxide (ZnO) nanoparticles from green algae and their assessment in various biological applications, Micromachines 14 (5) (2023) 928, https://doi.org/10.3390/mi14050928.

[56] M. Murali, C. Mahendra, Nagabhushan, N. Rajashekar, M.S. Sudarshana, K.A. Raveesha, K.N. Amruthesh, Antibacterial and antioxidant properties of biosynthesized zinc oxide nanoparticles from *Ceropegia candelabrum* L. – an endemic species, Spectrochim. Acta. A. Mol. Biomol. Spectrosc. 179 (2017) 104–109, https://doi.org/10.1016/j.saa.2017.02.027.

[57] B. Siripireddy, B.K. Mandal, Facile green synthesis of zinc oxide nanoparticles by *Eucalyptus Globulus* and their photocatalytic and antioxidant activity, Adv. Powder Technol. 28 (3) (2017) 785–797, https://doi.org/10.1016/j.apt.2016.11.026.

[58] Z.U.H. Khan, H.M. Sadiq, N.S. Shah, A.U. Khan, N. Muhammad, S.U. Hassan, K. Tahir, S.Z. safi, F.U. Khan, M. Imran, N. Ahmad, F. Ullah, A. Ahmad, M. Sayed, M.S. Khalid, S.A. Qaisrani, M. Ali, A. Zakir, Greener synthesis of zinc oxide nanoparticles using *Trianthema portulacastrum* extract and evaluation of its photocatalytic and biological applications, J. Photochem. Photobiol., B 192 (2019) 147–157, https://doi.org/10.1016/j.jphotobiol.2019.01.013.

[59] A. Sirelkhatim, S. Mahmud, A. Seeni, N.H.M. Kaus, L.C. Ann, S.K.M. Bakhori, H. Hasan, D. Mohamad, Review on zinc oxide nanoparticles: antibacterial activity and toxicity mechanism, Nano-Micro Lett. 7 (3) (2015) 219–242, https://doi.org/10.1007/s40820-015-0040-x.

[60] N. Padmavathy, R. Vijayaraghavan, Enhanced bioactivity of ZnO nanoparticles—an antimicrobial study, Sci. Technol. Adv. Mater. 9 (3) (2008) 1–7, https://doi.org/10.1088/1468-6996/9/3/035004.

[61] J.T. Seil, T.J. Webster, Antimicrobial applications of nanotechnology: methods and literature, Int. J. Nanomed. 7 (2012) 2767–2781, https://doi.org/10.2147/IJN.S24805.

[62] M.A. Ansari, M. Murali, D. Prasad, M.A. Alzohairy, A. Almatroudi, M.N. Alomary, A.C. Udayashankar, S.B. Singh, S.M.M. Asiri, B.S. Ashwini, H.G. Gowtham, N. Kalegowda, K.N. Amruthesh, T.R. Lakshmeesha, S.R. Niranjana, Cinnamomum verum bark extract mediated green synthesis of ZnO nanoparticles and their antibacterial potentiality, Biomolecules 10 (2) (2020) 336, https://doi.org/10.3390/biom10020336.

[63] M. Murali, S. Anandan, M.A. Ansari, M.A. Alzohairy, M.N. Alomary, S.M.M. Asiri, A. Almatroudi, M.C. Thriveni, S.B. Singh, H.G. Gowtham, M. Aiyaz, C. Srinivasa, A. Urooj, K.N. Amruthesh, Genotoxic and cytotoxic properties of zinc oxide nanoparticles phyto-fabricated from the *Obscure morning* glory plant Ipomoea Obscura (L.) ker Gawl, Molecules 26 (4) (2021) 891, https://doi.org/10.3390/molecules26040891.

[64] G. Sharmila, C. Muthukumaran, K. Sandiya, S. Santhiya, R.S. Pradeep, N.M. Kumar, N. Suriyanarayanan, M. Thirumarimurugan, Biosynthesis, characterization, and antibacterial activity of zinc oxide nanoparticles derived from *Bauhinia Tomentosa* leaf extract, J. Nanostructure Chem. 8 (3) (2018) 293–299, https://doi.org/10.1007/s40097-018-0271-8.

[65] J. Sawai, E. Kawada, F. Kanou, H. Igarashi, A. Hashimoto, T. Kokugan, M. Shimizu, Detection of active oxygen generated from ceramic powders having antibacterial activity, J. Chem. Eng. Jpn. 29 (4) (1996) 627–633, https://doi.org/10.1252/jcej.29.627.

[66] L. Zhang, Y. Jiang, Y. Ding, M. Povey, D. York, Investigation into the antibacterial behaviour of suspensions of ZnO nanoparticles (ZnO Nanofluids), J. Nanoparticle Res. 9 (3) (2007) 479–489, https://doi.org/10.1007/s11051-006-9150-1.
[67] M. Elshikh, S. Ahmed, S. Funston, P. Dunlop, M. McGaw, R. Marchant, I.M. Banat, Resazurin-based 96-well plate microdilution method for the determination of minimum inhibitory concentration of biosurfactants, Biotechnol. Lett. 38 (6) (2016) 1015–1019, https://doi.org/10.1007/s10529-016-2079-2.
[68] M. Anju, K. Balvinder, K. Rajesh, C. Dharvi, G. Mayukh, M. Mayank, B. Basanti, P. Yash, B.N. Tripathi, P. Minakshi, Metal/metal oxide nanoparticles: toxicity concerns associated with their physical state and remediation for biomedical applications, Toxicol Rep 8 (2021) 1970–1978, https://doi.org/10.1016/j.toxrep.2021.11.020.